International Journal of Minerals, Metallurgy and Materials
Volume 19, Number 4, Apr 2012, Page 333
DOI: 10.1007/s12613-012-0560-z

Microstructural evolution and mechanical properties of nanostructured Cu-Al-Ni shape memory alloys

M. Izadinia and K. Dehghani

Mining and Metallurgical Engineering Department, Amirkabir University of Technology, Tehran, Iran

(Received: 14 February 2011; revised: 10 October 2011; accepted: 13 October 2011)

Abstract: The melt spinning technique, with an applied cooling rate of about 10^6 K/s, was used to produce a nanostructured Cu+13.2Al+5.1Ni (in wt%) shape memory alloy. The properties of nanostructured ribbons were then compared with those of conventional coarse structure. The microstructural evolution was characterized using scanning electron microscopy (SEM), atomic force microscopy (AFM) and X-ray diffraction (XRD) techniques. Microhardness measurements indicate a two-fold increase in hardness because of the produced nanostructure. Comparing to its coarse structure, the nanostructured Cu-Al-Ni shape memory alloy exhibited the enhanced mechanical properties including a ductility of 6.5% and a pronounced plateau in the stress-strain curve.

Keywords: copper allosy; shape memory effect; melt spinning; mechanical properties; microstructural evolution

1. Introduction

1.1. Shape memory alloys (SMA)

The development of shape memory alloys (SMAs) began with Ni-Ti alloys followed by ternary Cu-based ones, e.g. Cu-Al-Ni, Cu-Zn-Al and Cu-Al-Be. Generally speaking, Cu-based shape memory alloys exhibit low mechanical properties and poor shape memory effect is attributed mostly to thier coarse grains [1-3]. Among Cu-based SMAs, Cu-Al-Ni alloys have a better thermal stability and are well suited for high temperature applications [4]. Cu-Al-Ni alloys produced by conventional casting techniques are brittle, which is attributed to their large elastic anisotropy and coarse grain size [5]. Therefore, improving the mechanical properties of Cu-Al-Ni shape memory alloys can be of significance in terms of their industrial applications. Thus, by modifying their microstructure, the mechanical properties of the Cu-based SMAs can be improved. Regarding the structural refinement of shape memory alloys, one practical approach is the rapid-solidification technique [6], which is studied in the present work.

1.2. Melt spinning technique

Rapid solidification is extensively used to modify the casting structure of materials. Among rapid-solidification methods, melt spinning (MS) is a well-known approach exhibiting unique advantages in refining the microstructure [7]. During melt spinning, a very high cooling rate of 10^5-10^7 K/s can be achieved readily [8]. In such a case, solidification can take place in milliseconds. Dehghani *et al.* [9-10] reported that, in the case of aluminum alloys, nanostructures produced by melt spinning exhibited: (i) a significant improvement in homogeneity and segregation, (ii) the appearance of metastable phases, (iii) a considerable fine dispersion of secondary phase, and (iv) an increase in solid solubility. As the size of grains at the polycrystalline material is reduced to nanoscale, the properties of nanostructured materials will be dominated by the fraction of grain boundary area. Thus, any changes in grain size can significantly affect the mechanical properties of materials.

In general, the higher the cooling rate during solidification, the finer the microstructure will be. Besides, by rapid solidification, some properties such as ductility and shape memory effect of Cu-Ni-Al alloys can be improved [11-13].

The aim of the present work was therefore to produce a nanostructured Cu-13.2%Al-5.1%Ni alloy by melt spinning. Then the effect of grain refinement on the mechanical prop-

Corresponding author: K.Dehghani E-mail: dehghani@aut.ac.ir

erties of nanostructured Cu-13.2%Al-5.1%Ni was investigated.

2. Experimental

The shape memory alloy (Cu-13.2%Al-5.1%Ni) used in the present study was prepared using a high-frequency induction furnace under argon atmosphere. Rectangular samples with dimensions of 60 mm × 30 mm × 0.9 mm were cut from the cast ingot. The specimens were then solution treated at 950°C (*i.e.* in β-phase region) for 1 h followed by water quenching to obtain an ordered metastable β phase. This is referred to as conventional coarse structure throughout the manuscript.

To produce the nanostructured Cu-13.2%Al-5.1%Ni, a melt spinning technique was used. The molten alloy was injected onto a rotating copper wheel of 280 mm in diameter. The highest wheel speed of 40 m/s was applied in order to attain the highest possible cooling rate, *i.e.* 10^7 K/s. The thickness of produced ribbons was about 20 μm. The melt-spinning process is schematically shown in Fig. 1.

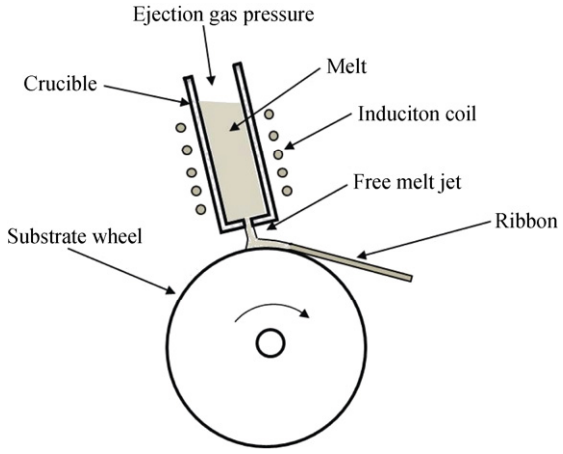

Fig. 1. A schematic of the melt spinning process.

The melt-spun specimens were etched using a solution consisting of 96% methanol, 2% HF and 2% $FeCl_3$. The microstructure of both the conventional coarse structure and the nanostructured ribbons were then characterized using a Philips-XL30 scanning electron microscope (SEM) equipped with an energy-dispersive X-ray analyzer. X-ray diffraction (XRD) were also used to identify the formed phases in both cases. The XRD studies were carried out using an X-Pert-Pro 2001 diffractometer with Cu K_α radiation at 40 kV and 20 mA. The angle was set at 2θ, ranging from 35° to 85°. The microstructure of melt-spun ribbons was also investigated using an atomic force microscope (AFM) (DME model, serial DS95).

The samples for mechanical tests were carefully prepared from the melt-spun ribbons in order to minimize defects, though the melt-spun ribbons are inherently non-uniform in shape. The microhardness was measured on different sections of the specimens using an applied load of 245 mN. In addition, the mechanical properties of the nanostructured and coarse-structure samples were compared using tensile testing.

3. Results and discussion

3.1. Microstructure

Fig. 2 illustrates an XRD pattern taken from the wheel side of the melt-spun ribbon. According to Fig. 2, phases in the structure can be identified as β_1 and β_1'. β_1 is an austenitic phase with a cubic structure, while martensitic β_1' phase has a monoclinic 18R structure. These are consistent with the results reported by other researchers [14]. The low intensity of β_1 peaks indicates that there is some untransformed austenite phase. No peaks related to the intermetallic phase of Cu, Al and Ni were observed. However, the absence of peaks concerning the intermetallic phases may not point out the absence of these phases. This can also be because the detection limit by the XRD technique is typically about 5vol% [15]. Thus, the absence of intermetallic peaks implies the extended solid solubility of elements such as Al and Ni in the matrix.

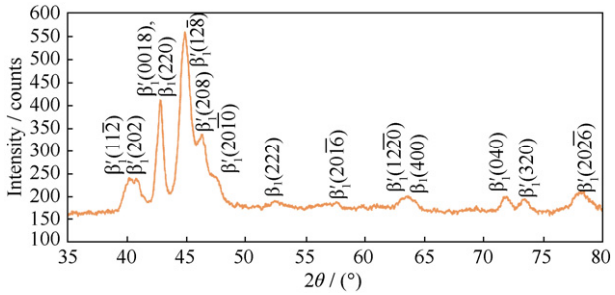

Fig. 2. XRD patterns of the wheel-side melt-spun ribbon.

The size of nanograins formed in the melt-spun ribbons was determined using the following equation [16]:

$$L=\frac{K\lambda}{\beta\cos\theta} \tag{1}$$

where K (≈0.89) is a constant that depends on the crystallite shape, λ is the wavelength (Cu K_α radiation), β is the full width at half maximum (FWHM) and θ is the Bragg angle. Using Eq. (1), the grain size (L) was determined to be about 70 nm for the wheel side of ribbons.

To calibrate the instrument, the LaB_6 single crystal was used, which should exhibit a peak with zero broadening. However, due to the instrumental effect, a 0.061 broadened peak was observed. To take into account this instrumental effect (0.061) on the observed broadening regarding nanograin and ultra fine grain specimen, the following equation is used:

$$\beta^2 = \beta_M^2 - \beta_S^2 \quad (2)$$

where β is the amount of broadening after considering the contribution of instrumental effect (β_S = 0.061) to the broadening obtained for the nanograin and ultra-fine grain sample (β_M = 0.32). This comes to a value of 0.314 for β. Thus, the contribution of instrumental effect to peak broadening is about 0.006, *i.e.* 0.32-0.314. Subtracting this amount (*i.e.* 0.006) from 0.32, the true value for the peak broadening with regards to the nanograin and ultra fine structure sample is 0.314. Therefore, the error concerning the instrumental effect is almost negligible in the present case.

Fig. 3 shows the SEM micrograph of the sample solution-treated at 950°C for 1 h followed by water quenching. It can be seen that the alloy is in martensitic state at room temperature. According to Fig. 3, the martensitic β_1' is formed in the solution-treated sample which has the typical zigzag morphology.

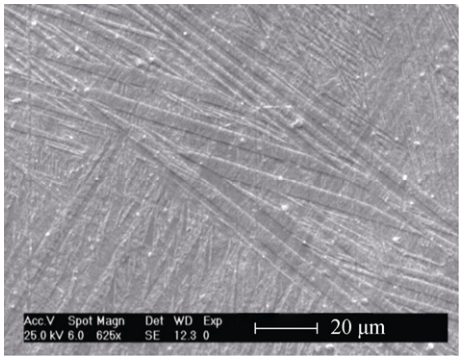

Fig. 3. SEM micrograph of the conventional solution treated sample at 950°C for 1 h and water quenched at room temperature.

Referring to Fig. 4, different grains exhibit different orientations. For example, the V-shape martensite is formed in some regions, while in other areas within the matrix, needle-like martensite is observed.

Figs. 5 and 6 compare precipitates formed in the conventional structure and in the melt-spun ribbons. The compositions

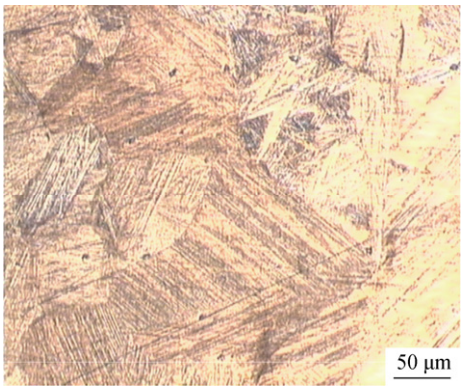

Fig. 4. Optical microstructures of the solution treated alloy that showing grain boundaries and various martensitic variants orientation.

of these particles were determined using energy dispersive X-ray (EDX) analysis. Figs. 5(b) and 6(b) present the EDX results regarding the formed phases. The characteristics of the patterns and the peaks confirm the presence of Cu_9Al_4 precipitates. Besides, the SEM image presented in Fig. 6(a) indicates the formation of nanoparticle γ_2 (Cu_9Al_4) during melt spinning. The composition of nanoparticles presented in Fig. 6(b) confirms that although Ni exists in the EDX analysis, its concentration is lower than the bulk concentration of Ni. In fact, it is very likely that the EDX analysis of nanoparticles is influenced by the background concentration.

Referring to Fig. 6(a), the radius of nanoparticles is about

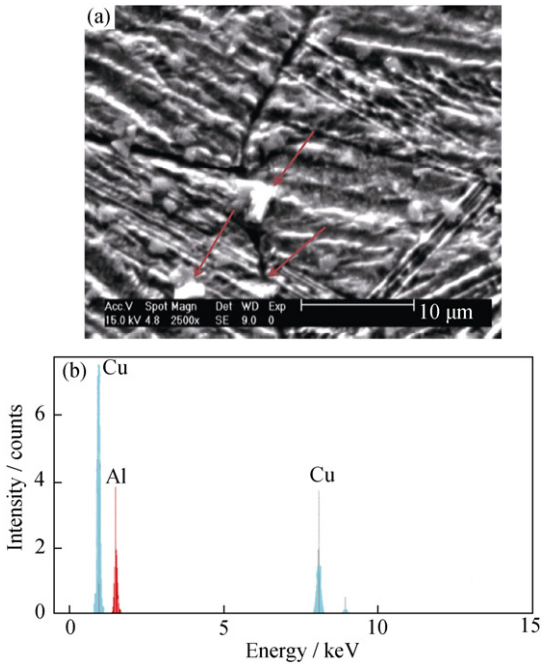

Fig. 5. SEM micrograph of the conventional structure indicating microsize γ_2 precipitates (a) and related EDX patterns (b).

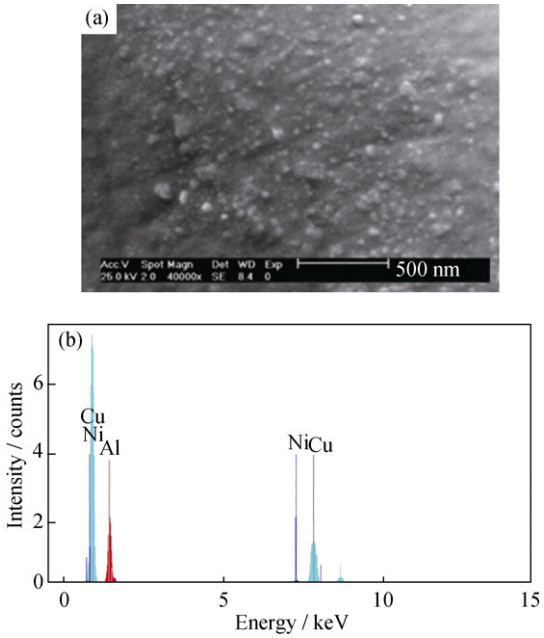

Fig. 6. SEM micrographs of melt-spun foils indicating nanosize γ_2 precipitates (a) and related EDX patterns (b).

25 nm. They are finely dispersed with a spacing of approximately 300 nm.

One important issue regarding the nanostructured materials is their thermal stability. Thus, the large driving force due to the high volume fraction of grain boundaries can cause the structure instability of nanograin materials. This instability can result in grain growth leading to the degradation of superior properties attributed to nanograin structures. Fine dispersed second-phase particles prevent the motion of grain boundaries by exerting a pinning pressure. This phenomenon is known as Zener pinning, which is important because of its strong influence in preventing the grain boundary migration. In the present work, the formation of γ_2 (Cu_9Al_4) nanoparticles can pin the grain boundaries and prevent their motion during thermal cycles. Particles in the conventional structure are too coarse (about to 0.8 μm) to exert Zener drag. Compared to the conventional structure, the presence of nanoprecipitate of γ_2 (25 nm) in the melt-spun ribbons results in the thermal stability of the microstructure by preventing the motion of high-angle grain boundaries. The particle spacing (δ) can be calculated as follows [17]:

$$\delta=\frac{4(1-f)r}{3f} \tag{3}$$

where r and f are the radius and volume fraction of particles, respectively. As f has the same value for the both conventional and nano-structure melt-spun ribbons, the ratio of inter-particle spacing of nanostructure (δ_{ns}) to conventional structure (δ_{cs}) will be derived from

$$\frac{\tau_{ns}}{\tau_{cs}}=\frac{r_{ns}}{r_{cs}} \tag{4}$$

where r_{ns} and r_{cs} are the radius of γ_2 particles in the nanostructured and conventional structure, respectively. Referring to Figs. 5 and 6, the average radius of γ_2 particles (r_{ns}) measured from the SEM micrograph is about 25 nm, while the value for the conventional structure is about 0.8 μm. Therefore, the value of δ_{cs}/δ_{ns} will be about 32. Considering the shear stress required for a dislocation to overcome the barrier between two γ_2 particles as

$$\tau\propto\frac{1}{\delta} \tag{5}$$

Hence,

$$\frac{\tau_{ns}}{\tau_{cs}}=\frac{\delta_{cs}}{\delta_{ns}} \tag{6}$$

where τ_{ns} and τ_{cs} are respectively the shear stresses for the nanostructured and coarse structure cases. Substituting the amount of δ_{cs}/δ_{ns} ratio in Eq. (6), the value of τ_{ns}/τ_{cs} will also be about 32. This means that the shear strength of the nanostructured Cu-Al-Ni ribbon can be about 32 times higher than that of the conventional structure. In other words, the formation of nanograins and nanoparticles of γ_2 (Cu_9Al_4), with nano-interparticle spacing can lead to significant increases in the mechanical properties of produced ribbons/foils. Such an enhanced increase in the properties of the nanostructured Cu-Al-Ni alloy, produced by melt spinning, is consistent with past works [18-20].

The nanostructure of the as-spun Cu-Al-Ni ribbon was investigated by AFM to confirm the formation of nanograins and ultra fine grains. AFM images taken from the surface of the studied Cu-Al-Ni ribbon are presented in Fig. 7. These micrographs confirm clearly the formation of nanograins and ultra fine grains ranging between 70 and 150 nm.

In another approach, the formation of nanograins was investigated by the SEM technique. Fig. 8 shows the SEM micrograph indicating the formation of nanograins during melt spinning.

3.2. Mechanical properties

The microhardness values of the nanostructure and coarse-

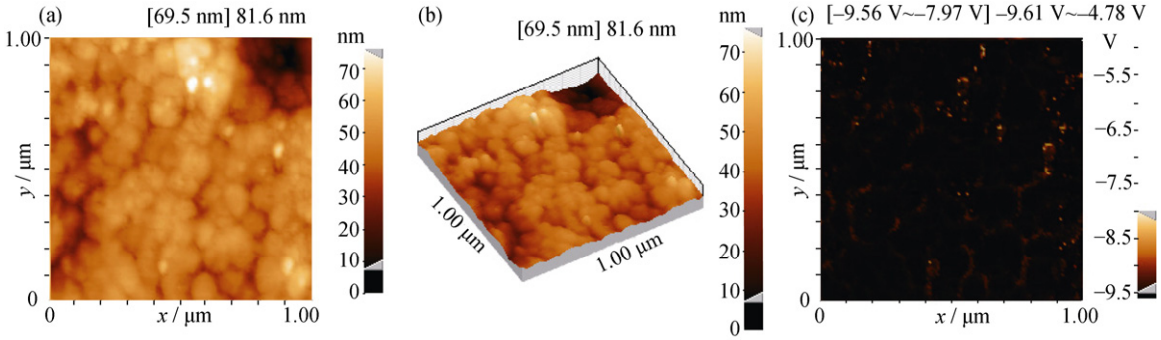

Fig. 7. AFM micrographs taken from nanograins and ultra fine grains formed in the surface of the as-spun ribbon (scan setup direction 0°, force 0.7 nN): (a) 2D topography; (b) 3D topography; (c) phase.

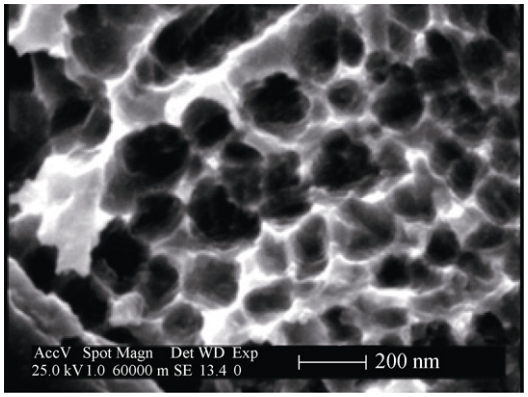

Fig. 8. SEM image of th melt-spun ribbon showing nanograins formed during rapid solidification.

structure cases are summarized in Table 1. From this table, the average hardness of the conventional structure Cu-Al-Ni alloy is about 217 HV, while that of the melt-spun ribbon is approximately 450 HV. These results are in good agreement with those reported by other researches [21]. As rapid solidification leads to a considerable reduction in grain size, this consequently results in an increase in hardness. This indicates that the microhardness of the melt-spun nanostructure is about twice that of a conventional one. The enhanced microhardness can be attributed to the formation of γ_2 nanoparticles as well as to the decrease in grain size to nanoscale; both are unique characteristics of the present nanostructure produced by melt spinning.

Table 1. Vickers hardness (HV) of the melt-spun ribbons and conventional samples of the Cu-Al-Ni alloy

Value of each sample		Average value	
Conventional structure	Melt-spun	Conventional structure	Melt-spun
225.2 ± 3.4	441 ± 3.4		
234 ± 3.1	446 ± 3.6		
210 ± 2.9	453 ± 3.8	216.9±3.3	449.6±3.6
205.4 ± 4.2	465 ± 4.1		
210 ± 2.7	443 ± 3.1		

The stress-strain curves obtained by tensile testing are illustrated in Fig. 9. According to this figure, the stress-strain response of the Cu-Al-Ni alloy changes with grain refining. The properties measured from the stress-strain curves are summarized in Table 2. The stress-strain curve of the present Cu-Al-Ni alloy shows the common features of shape memory alloys, *i.e.* a distinct elastic region followed by a plateau and a hardening region. The characteristics of the plateau region can be used to determine the controlling mechanisms, e.g. the deformation-induced martensitic transformation and reorientations of martensitic variants. In fact, the stress-induced growth of martensite in one orientation occurs at the

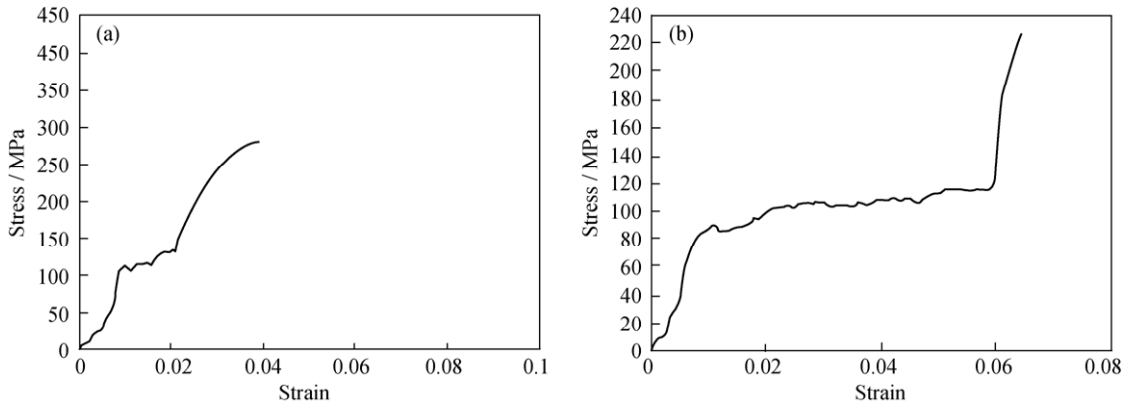

Fig. 9. Stress-strain curves obtained from tensile tests performed on the alloys: (a) conventional sample; (b) melt-spun ribbon.

Table 2. Property results obtained from tensile tests

Alloy	Yield stress / MPa	Ultimate tensile strength (fracture stress) / MPa	Maximum strain (fracture strain) / %
Conventional structure	120±10	230±10	4
Melt-spun ribbon	90±10	280±10	6.5

expense of the growth of adjacent plate-oriented martensite. During the hardening stage, the generation of dislocations and the growth of some martensitic variants take place.

In the case of the melt-spun specimen, the stress-strain curve exhibits a much longer plateau. This can be attributed to the refining of martensitic variants along with the formation of nanograins. Fine martensitic variants can more easily reorient with the applied stress.

On the other hand, the much smaller plateau region in the case of coarse structure samples can be due to the occurrence of premature fracture because of coarse grains. The premature failure is pronounced not only by coarse grains but also by grain boundary segregation [22]. In the nanostructured Cu-Al-Ni shape memory alloy, with increasing the plateau region, one can attain more shape memory effect.

Comparing the tensile behavior of the nanostructured Cu-base shape memory alloy with its coarse-structured counterpart, the tensile strength of the former was smaller than that of the latter. Although this was unexpected, it can be more likely due to the very thin specimens and the non-uniform edges of specimens in case of the nanostructured sample.

4. Conclusions

The structure and mechanical properties of nanostructured and ultra fine structured Cu-Al-Ni SMAs are compared with those of the coarse structured. The nanostructure and ultra fine structure of Cu-Al-Ni SMAs exhibit unique properties compared to their coarse grain counterparts. The produced nanostructure resulted in enhanced mechanical properties. The hardness of nanostructured Cu-Al-Ni SMAs can be as much as twice that of the conventional coarse structured. Besides, nanoparticles produced by melt spinning can exhibit significant effect on the structure stability of nanostructured Cu-Al-Ni obtained by rapid solidification.

References

[1] R. Wang, J. Gui, X. Chen, and S. Tan, EBSD and TEM study of self-accommodating martensites in $Cu_{75.7}Al_{15.4}Mn_{8.9}$ shape memory alloy, *Acta Mater.*, 50(2002), p.1835.

[2] K. Otsuka, H. Sakamoto, and K. Shimizu. Successive stress-induced martensitic transformations and associated transformation pseudoelasticity in Cu-Al-Ni alloys, *Acta Metall.*, 27(1979), p.585.

[3] K. Sugimoto, K. Kamei, H. Matsumoto, S. Komatsu, K. Akamatsu, and T. Sugimoto, Grain-refinement and the related phenomena in quaternary Cu-Al-Ni-Ti shape memory alloys, *J. Phys. Paris Colloq.*, 43(1982), p.761.

[4] G.S. Yang, J.K. Lee, W.Y. Jang, S.J. Jeong, and K. Inoue, Effect of aging and microstructure on mechanical rolling CuAlNi shape memory alloy, *Mater. Sci. Forum*, 539-543(2007), p. 3326.

[5] C.Y. Chung and C.W.H. Lam, Cu-based shape memory alloys with enhanced thermal stability and mechanical properties, *Mater. Sci. Eng. A*, 273-275(1999), p.622.

[6] X. Zhang and A. Atrens, Rapid solidification characteristics in melt spinning, *Mater. Sci. Eng. A*, 159(1992), p.243.

[7] H.H. Liebermann, *Rapidly Solidified Alloys: Processes, Structures, Properties, Applications*, CRC Press, New York, 1993, p.254.

[8] T.R. Anantharaman and C. Suryanarayana, *Rapidly Solidified Metals*, Trans Tech Publications, Switzerland, 1987, p.5.

[9] K. Dehghani, M. Salehi, M. Salehi, and H. Aboutalebi, Comparing the melt-spun nanostructured aluminum 6061 foils with conventional direct chill ingot, *Mater. Sci. Eng. A*, 489(2008), p.245.

[10] M. Salehi and K. Dehghani, Structure and properties of nanostructured aluminum A413.1 produced by melt spinning compared with ingot microstructure, *J. Alloys Compd.*, 457(2008), p.357.

[11] Y. Sutou, R. Kainuma, and K. Ishida, Effect of alloying elements on the shape memory properties of ductile Cu-Al-Mn alloys, *Mater. Sci. Eng. A*, 273-275(1999), p.375.

[12] M.A. Morris, Influence of boron additions on ductility and microstructure of shape memory Cu-Al-Ni alloys, *Scripta Metall. Mater.*, 25(1991), p.2541.

[13] M.A. Morris, High temperature properties of ductile Cu-Al-Ni shape memory alloys with boron additions, *Acta Metall. Mater.*, 40(1992), p.1573.

[14] T. Saburi and C.M. Wayman, Crystallographic similarities in shape memory martensites, *Acta Metall.*, 27(1979), p.979.

[15] N. Ünlü, A. Genç, M.L. Öveçoğlu, N. Eruslu, and F.H. Froes, Characterization investigations of melt-spun ternary Al-*x*Si-3.3Fe (x=10, 20 wt.%) alloys, *J. Alloys Compd.*, 322(2001), p.249.

[16] B.D. Cullity, *Elements of X-Ray Diffraction*, Vol.1, 2nd Ed, Addison-Wesley Publishing Company, Massachusetts, 1978, p.87.

[17] G.E. Dieter, *Mechanical Metallurgy*, McGraw-Hill Series, New York, 1976, p.68.

[18] S. Zeller and J. Gnauk, Shape memory behavior of Cu-Al wires produced by horizontal in-rotating-liquid-spinning, *Mater. Sci. Eng. A*, 481-482(2008), p.562.

[19] J. Malarría, C. Elgoyhen, P. Vermaut, P. Ochin, and R. Portier, Shape memory properties of Cu-based thin tapes obtained by rapid solidification methods, *Mater. Sci. Eng. A*, 438-440(2006), p.763.

[20] H. Morawiec, J. Lelatko, D. Stróz, and M. Gigla, Structure and properties of melt-spun Cu-Al-Ni shape memory alloys, *Mater. Sci. Eng. A*, 273-275(1999), p.708.

[21] S. Amelinckx and W. Dekeyser, The structure and properties of grain boundaries, *Solid State Phys.*, 8(1959), p.325.

[22] U. Sari, Influences of 2.5wt% Mn addition on the microstructure and mechanical properties of Cu-Al-Ni shape memory alloys, *Int. J. Miner., Metall. Mater.*, 17(2010), p.192.